

SMALL CRACK TEST PROGRAM FOR HELICOPTER MATERIALS *

Bal Annigeri
United Technologies Research Center
East Hartford, CT

George Schneider
United Technologies, Sikorsky Aircraft
Stratford, CT

52-39

23096

R 16

ABSTRACT

Crack propagation tests were conducted to determine crack growth behavior in five helicopter materials for surface cracks between 0.005 to 0.020 inches in depth. Constant amplitude tests were conducted at stress ratios $R = 0.1$ and 0.5 , and emphasis was placed on near threshold data (i.e. 10^{-8} to 10^{-6} inches/cycle). Spectrum tests were conducted using a helicopter spectrum.

The test specimen was an unnotched tension specimen, and cracks were initiated from a small EDM notch. An optical/video system was used to monitor crack growth. The material for the test specimens was obtained from helicopter part forgings. Testing was conducted at stresses below yield to reflect actual stresses in helicopter parts.

INTRODUCTION/BACKGROUND

At the present time helicopters are generally "Safe Life" designed and maintained. This means that conservative structural component replacement times are defined based on SN fatigue data, and parts are removed at these replacement times. Inspections may be performed at periodic intervals based on experience with service problems such as wear and corrosion.

The Air Force damage tolerance approach, in which inspection intervals are quantified through crack growth analysis, has been applied to some helicopter structures to define inspection intervals in instances of service problems. Sikorsky Aircraft has also been investigating the general application of damage tolerance to the H-53 helicopter under Air Force contracts.

* Test program performed by United Technologies Sikorsky Aircraft and Research Center under contract F09603-89-G-0096-0014.

As part of the Air Force damage tolerance investigations crack propagation data was generated for the actual materials used in the H-53. Initial crack propagation data was obtained for large cracks using compact tension specimens, and for somewhat smaller corner cracks (greater than 0.015 inches) using edge notch specimens.

This crack propagation data was then used to assess crack growth times and inspection intervals in H-53 rotor and airframe structure. These structures are subjected to significant vibratory loading at frequencies of the main and tail rotor rpm (approximately 3 and 12 hz, respectively), and sometimes at two to four times these frequencies. As a result crack growth analyses often involved initial crack depths at the limit of detectability (0.005 inches); and, even at these small crack sizes, crack growth times in some structures were relatively short.

One concern in these crack growth assessments was the validity of the crack growth rate data at crack depths as small as 0.005 inches. A test program was therefore conducted under Air Force funding with the objective of obtaining crack growth rate data for surface cracks between 0.005 and 0.020 inches in depth in H-53 dynamic system and airframe materials. Emphasis was placed on constant amplitude near threshold data (i.e. 10^{-8} to 10^{-6} inches/cycle). Some spectrum testing was also performed to examine load interaction effects.

MATERIAL SELECTION AND DESCRIPTION

Five materials were chosen for the test program based on a survey of materials in primary H-53 rotor and airframe structure. The materials are as follows:

1. Al7075-T73 forging
2. 4340 (150 ksi) steel forging
3. Ti-6Al-4V alpha-beta forged, annealed
4. Ti-6Al-4V alpha-beta forged, solution heat treated and annealed
5. Ti-6Al-4V beta STOA forged

These materials encompass most of the H-53 structure, and are also common in many other Sikorsky helicopters such as the H-60 series (Black Hawk, Sea Hawk, and Night Hawk). The Al7075-T73 forgings are used in a number of main and tail rotor parts, and most of the major frames and fittings in the airframe are fabricated from this material. The 4340 steel and three titaniums are used primarily in main and tail rotor parts.

All the materials are die forgings and they were all obtained from actual helicopter parts bought to Sikorsky specifications as

indicated in Table 1. Conformance to the specifications was verified through standard Sikorsky materials process evaluations. The use of actual parts for material sources was considered essential in providing proper material form, microstructure, and properties.

Tensile ultimate and yield strengths for the materials are provided in Table 2. The Al7075-T73 and 4340 steel properties are "S" basis design properties from Mil-Hdbk-5E. The titanium properties are the average of the properties measured in the Sikorsky material conformance tests.

EXPERIMENTAL METHODS

The test facility at the United Technologies Research Center (Fig. 1) consists of a 3310 series "Interlaken" test system which includes a fully automated servo-hydraulic, closed loop test machine and a model 3200 controller. A Universal Test Program Series 3110, which is a menu driven software system, was used to control the test under both constant amplitude and spectrum loading.

Crack Detection And Monitoring

An optical/video crack detection and monitoring system was selected and developed for this program. This method was selected over other methods such as replicate (refs. 1,2) and electric potential drop (ref. 6) based on efficiency in developing the test procedures and performing the tests. Similar optical methods for crack detection using a camera instead of a video system had been successfully used in references 3,4, and 5. The major components in this system consisted of a macrophoto lens, a CCD video camera, video recorder, strobed fiber optic lighting, and a video monitor. The use of a strobed lighting system provided the ability to capture the image of the crack at the maximum load without stopping the tests. It was therefore possible to video monitor and record the crack growth in real time. Crack lengths were measured on the video monitor which was calibrated against measurements taken in the microscope. The crack length measurements were taken as the projected crack length along a straight line in the crack direction.

Specimen Configuration

In the selection of the test specimen the two types shown in Figure 2 (refs 1,2,4,5) were considered. Both of these specimens provided small test sections which facilitated the detection and tracking of naturally initiated cracks. As shown in Fig 2a the

notched specimen (refs. 1,2) consists of single edge notch plate with overall dimensions of 12 x 2 inches and a semicircular notch of radius of .125 inches. The unnotched specimen in Figure 2b (refs. 4,5) is a smoothly tapered specimen, and therefore it has no significant stress concentration. Its overall dimensions are 6 x 0.3 inches. Although both specimens appeared reasonable, the unnotched specimen was chosen for the following reasons:

1. The smaller overall specimen size facilitated specimen manufacture from actual helicopter parts.
2. It would not have to be stabilized at $R = -1$ testing as would the larger notched specimen.
3. It had no stress concentration. This results in a simpler stress intensity solution. It was also believed that the notched specimen might require higher stresses at the crack origin to naturally initiate a crack.

The regions of the specimen in which cracks initiated were manufactured to minimize residual stresses and provide a surface suitable for visualization of small cracks. The specimen preparation involved an initial EDM process to form the taper shape in the gage section. The specimens were then hand polished with a 240 to 320 grit wet sand paper to remove the EDM remelt and heat affected areas. The next step was chemical milling of the steel and titanium specimens and electro polishing of the aluminum specimens. The final preparation involved wet sanding with 600 to 1000 grit sand paper, and then polishing with 30, 15 and 3 micron diamond paste in a Varsol solution.

Test Method Development

The test method development consisted of modifications to the specimen geometry, surface preparation, optical magnification, and specimen lighting. The specimen geometry was modified to that shown in Figure 3 to lower grip loads and thus prevent slip and failure at the grips. It was also determined that highly polished surfaces, and specialized fiber optic lighting were necessary for tracking the crack. In early testing, naturally initiated cracks were attempted using a 30X magnification. However, problems in detecting the crack led to a final magnification of 200x, and the use of a very small EDM starter notch to facilitate and localize crack initiation. Very small EDM notches (0.006 to 0.009 inch surface lengths) were achieved by introducing an initial EDM notch, and then polishing the specimen to reduce the notch size.

EXPERIMENTAL PROGRAM

Test Plan

The test plan was to perform eight tests for each of the five selected H-53 materials. These tests consisted of two constant amplitude tests at each of three stress levels $R = \sigma_{\min}/\sigma_{\max} = -1, 0, \text{ and } 0.5$ and two spectrum tests. Due to budget and technical constraints the $R = -1$ tests were not performed. The objective was to provide crack growth rate data for surface cracks from 0.005 to 0.020 inches in depth in the near threshold region. It was desired that the cracks be naturally initiated to obtain the best possible data, but, as noted, it was necessary to use small EDM starter notches. Another important consideration was to perform the tests for stresses below yield to reflect stress levels typical of helicopter structure.

Stress Intensity Considerations

One of the problems in the test program was to perform propagation tests for 0.005 to 0.020 depth cracks at low stress intensity values. The problem is illustrated in Table 3. This table shows the maximum stresses (based on Sikorsky SN data) needed to initiate a crack in a reasonable number of cycles (0.5 to 1 million); the stress intensity ranges ΔK at these stress levels and crack depths of 0.005, 0.010, and 0.020; and the large crack threshold stress intensities. As shown the stress intensities at the crack sizes of interest are all well above the large crack thresholds.

The method used to overcome this problem for stress ratios $R = 0$ and $.5$ was to initiate the crack at $R = -1$ (compression fatigue) as suggested in reference 4. If the crack propagation tests are then performed at $R = 0$ and 0.5 without changing the maximum stress, lower ΔK 's than those in Table 3 may be realized. Using this method ΔK values near the large crack threshold were obtained for $R = 0$ and 0.5 . However, no solution was obtained for $R = -1$.

Another possibility for obtaining lower stress intensities is that the EDM starter notch might reduce the stress required for crack initiation from those shown in Table 3. However during the development testing it was found that even with the EDM notch it was difficult to initiate cracks at stresses much below those in the table.

Spectrum Considerations

A number of helicopter stress spectra were examined for use in the spectrum crack growth tests. These spectra included the two standard helicopter rotor spectra HELIX28 and FELIX32 which were developed in a European collaborative effort for hinged and fixed rotor systems, respectively. Three spectra used in Sikorsky crack propagation assessments of the H-53 were also examined. These spectra included those for the airframe pylon fold hinge, the main rotor spindle (blade retention component), and the outboard blade spar.

Significant variability was found in these spectra. The HELIX32 spectrum showed very little variation in maximum stress and its predominate stresses (stresses at which most cycles occur) are at $R = 0.4$. The FELIX28 spectrum has overloads in maximum stress around 1.5 times the predominate stresses, and its predominate stresses are at $R = 0.1$ to 0.3 . The H-53 pylon fold spectrum has overloads in maximum stress of 1.2 to 2.4 times the predominate stresses, and its predominate stresses are at R values of 0.6 to 0.8 . The H-53 main rotor spindle has little variation in maximum stress, and its stress ratios are mostly between 0.7 and 0.8 . The H-53 main rotor outboard blade spectrum has the most variability in maximum stress of all the spectra examined with some overloads as high as 3 to 4 times the predominate stress levels. The outboard blade spectrum has a wide range of R values from 0.1 to 0.6 for high frequency stresses.

In this test program a modified H-53 pylon fold spectrum was selected for use in the spectrum tests. The spectrum was modified to maintain all R values below 0.6 . This spectrum is representative of helicopter spectra with reasonably high overload factors.

TEST DATA AND TEST RESULTS

Table 4 provides a summary of the constant amplitude tests performed. At least two constant amplitude tests were performed for each of the five materials at stress ratios $R = 0.1$ and 0.5 . The cracks were initiated from the EDM notch in compression fatigue ($R = -1$), and the maximum stress was either maintained or slightly increased for the crack propagation testing at $R = 0.1$ or 0.5 . As explained, the initiation of cracks at $R = -1$ resulted in lower stress intensities than could be achieved by initiating the cracks at positive R ratios. The maximum stress is maintained the same for crack propagation to avoid overload effects.

Table 5 provides a summary of the spectrum tests performed. One spectrum test was performed for each material using the H-53 airframe pylon fold spectrum. The cracks were initiated using

constant amplitude compression fatigue ($R = -1$). As shown in the table the maximum crack initiation stress was well below the maximum spectrum stress, and it was even below some of the high cycle maximum stresses in the spectrum.

Crack length (a) versus cycle data (N) was recorded using the calibrated optical/video system for each constant amplitude and spectrum test. The constant amplitude data was converted to crack propagation rate data (da/dN vs ΔK) using the ASTM secant method for determining da/dN , and a simple infinite plate solution for stress intensity K . The infinite plate solution assumes a semicircular crack, and examination of the fracture surface verified that this was a reasonable assumption. The mathematical expressions are:

$$da/dN = (a_{i+1} - a_i) / (N_{i+1} - N_i)$$

and

$$K = 0.7\sigma(\pi a)^{1/2}$$

At the present time a limited amount of data analysis has been performed for the constant amplitude test. The results for $R = 0.1$ are plotted in Figures 4 through 7. In all but Figure 4 (Al7075-T73) the small crack data is compared with large crack compact tension test data obtained about eight years ago in another Air Force funded test program. The Al7075-T73 is compared with large crack propagation rate curves used in the crack propagation computer program FLAGRO.

The Al7075-T73 $R = 0.1$ crack growth rate data (Fig 4) shows considerable scatter. The Al-2 specimen shows the most reasonable behavior with generally increasing da/dN with ΔK . The Al-16-1 and Al-3 specimens show erratic crack growth behavior. The Al-16-1 specimen generally showed a decreasing da/dN with increasing ΔK . This may be due to the small initial crack size (Table 4) and interaction with the EDM notch. The Al-3-1 specimen was tested at the highest ΔK values and its behavior is also erratic. The Al-2 test specimen shows reasonable agreement with the FLAGRO curve.

Some preliminary evaluation of the Al7075-T73 $R = 0.5$ data shows good agreement between the two specimens. The crack propagation rate da/dN is also generally increasing with increasing ΔK , but there is still a considerable amount of data scatter.

The 4340 steel $R = 0.1$ crack growth rate data (Fig 5) shows much less scatter than the aluminum, and remarkable agreement with the large crack compact tension threshold test results conducted eight years ago. The material sources for both the small and large crack specimens were H-53 main rotor hinge pins, but separate forgings were purchased from inventory and heat treated eight years apart.

The Ti-6Al-4V beta STOA small crack $R = 0.1$ data is shown in Figure 6 along with large crack compact tension threshold test data. The small crack data shows considerable scatter, and faster crack propagation rates than the large crack data. The material sources for the large and small crack specimens were a UH-60 main rotor retention spindle forging, and a large H-53 elastomeric main rotor hub forging, respectively.

The Ti-6Al-4V alpha-beta $R = 0.1$ small crack data is shown in Figure 7, along with large crack compact tension threshold test data. As with the 4340 steel the Ti-6Al-4V alpha-beta crack growth rate data shows little scatter, and excellent agreement between large and small cracks. The small crack data contains both annealed and solution heat treated and annealed forgings, and shows no difference in their crack growth rates. The large crack specimens were obtained from a large H-53 conventional main rotor hub forging, and the small crack specimens were obtained from smaller retention components (Table 1).

CONCLUSIONS

This test program has provided constant amplitude and spectrum crack propagation data for small surface cracks 0.005 to 0.020 inches in depth for five common helicopter forged materials. The test specimens were obtained from helicopter part forgings, and the materials were checked against Sikorsky material conformance specifications. The tests were conducted at stresses well below the yield stress to be representative of stresses in helicopter parts.

Preliminary analysis of the constant amplitude test data indicates that the 4340 steel and Ti-6Al-4V alpha-beta data show little crack growth rate data scatter when using the ASTM secant method to calculate da/dN . These materials also showed good agreement with large crack compact tension threshold test data. The Al7075-T73 and Ti-6Al-4V beta STOA materials show considerable data scatter when using the ASTM secant method to calculate da/dN . The aluminum data showed erratic behavior possibly due to interaction with the EDM notch. The Ti-6Al-4V beta STOA data tended to show faster crack propagation rates than that from large crack compact tension specimens.

Further data analysis needs to be performed to evaluate the constant amplitude $R = 0.5$ and spectrum data, and to compare this with other Air Force funded test program data for helicopter materials. These other test programs include the compact tension data referenced in this paper, and some notched specimen corner crack data for initial crack radii between 0.015 and 0.030 inches. Other methods for crack growth rate calculations should be evaluated, such as the modified polynomial regression technique (refs. 4 and 5).

Further testing is recommended to obtain naturally initiated crack propagation data to avoid possible interaction with the EDM starter notch, and to perform tests at $R = -1$. It is also recommended that tests be performed at lower stress intensities to determine if 0.005 inch deep cracks will grow below the large crack threshold.

Performing tests at lower stress intensities and at $R = -1$ for 0.005 to 0.020 inch deep cracks is a difficult problem. A load shedding test was performed for one of the constant amplitude $R = 0.1$ Al-7075-T73 specimens (specimen Al-16). In this test the loads were shed abruptly, and the data indicates that the crack propagated below the large crack threshold. The crack growth rates (da/dN) calculated by the secant method showed considerable data scatter.

ACKNOWLEDGEMENTS

The work in this report was funded by the U.S. Air Force under contract no. F09603-89-G-0096-0014 to Sikorsky Aircraft with Mr. Gary Chamberlain of Warner Robins ALC as the program manager. This support is gratefully acknowledged. Thanks are also due to L. H. Favrow for directing the test program, R.I. Holland for performing the tests, P. Inguanti for material conformance evaluations, R.J. Haas for assistance in selection and design of the optical/video system, and M. Winter and J. Wegge for development of computer image processing.

REFERENCES

1. Edwards, P.R. and Newman J.C. Jr., Short-Crack Growth Behavior in Various Aircraft Materials, AGARD Report No. 767, August 1990.
2. Newman, J.C., Jr, and Edwards, P.R., Short-Crack Growth Behavior in an Aluminum Alloy -An AGARD Cooperative Test Programme, AGARD Report No. 732, December 1988.
3. Iyyer, N.S. and Dowling, E., Fatigue Growth and Closure of Short Cracks, AFWAL-TR-89-3008, June 1989. (VPI)
4. Larsen, J.M., The Effects of Slip Character and Crack Closure on the Growth of Small Fatigue Cracks in Titanium-Aluminum Alloys, WRDC-TR-89-4094, February 1990.
5. Larsen, J.M., et. al., Measurement of Small Cracks by Photomicroscopy: Experiments and Analysis, ASTM STP 1149, 1992.
6. Hudak, S.J.Jr., and Bucci, R.J., Fatigue Crack Growth Measurement and Data Analysis, ASTM STP 738, 1979.

Table 1. Materials For Small Cracks Program

Material	Source	Part Number/Quantity
Al7075-T73 Die Forging	SH-60 STA 295 Side Fuselage Frame	70209-222054-002 1
Steel 4340 (150 ksi) Die Forging	H-53 Main Rotor Horizontal Hinge Pin	65103-11020-006 2
Ti-6Al-4V Beta STOA Die Forging	H-53 Main Rotor Elastomeric Hub	65103-11501-103 1
Ti-6Al-4V Alpha-Beta Die Forging, Annealed	H-53 Main Rotor Hub	65102-11541-002 2
Ti-6Al-4V Alpha-Beta Die Forging, Solution Heat Treated and Annealed	S-76 Main Rotor Spindle/Cuff	65102-11541-002 1

Table 2. Material Properties

Material	Ultimate (ksi)	Yield (ksi)
Al7075-T73 Die Forging	66	54
Steel 4340 (150 ksi) Die Forging	150	132
Ti-6Al-4V Beta STOA Die Forging	133	145
Ti-6Al-4V Alpha-Beta Die Forging, Annealed	139	129
Ti-6Al-4V Alpha-Beta Die Forging, Solution Heat Treated and Annealed	155	147

Table 3. Fatigue Stresses and Threshold Stress Intensity Factor

Material	R Ratio	Fatigue Vibratory Stress (ksi) for Initiation in 0.5 to 1.0 x 10 ⁶	ΔK (ksi ($\sqrt{\text{in}}$))			Large Crack ΔK_{th} (ksi ($\sqrt{\text{in}}$))
			$a = .005 \text{ in}$	$a = .01 \text{ in}$	$a = .02 \text{ in}$	
Al7075-T73 Forged	-1	29-34	5.1-6.0	7.2-8.4	10.1-11.9	
	0.0	20-22	3.5-3.9	5.0-5.5	7.0-7.7	2.5-3.5
	0.5	13-14	2.3-2.5	3.2-3.5	4.6-4.9	1.5-2.2
Steel 4340 (150 ksi) Forged	-1	70-74	12.3-13.0	17.3-18.3	24.6-26.0	
	0.0	58-60	10.2-10.5	14.4-14.9	20.4-21.0	4-7
	0.5	35-36	6.1-6.3	8.7-8.9	12.2-12.6	3-4
Ti-6Al-4V Beta STOA Forged	-1	80-85	14.0-14.9	19.8-21.1	28.0-29.8	
	0.0	55-59	9.7-10.4	13.6-14.6	19.3-20.7	4.6
	0.5	34-35	6.0-6.1	8.4-8.7	11.9-12.3	2.5-4.0
Ti-6Al-4V Alpha-Beta Forged	-1	40-60	7.0-10.5	9.9-14.9	14.0-21.0	
	0.0	30-50	5.3-8.7	7.4-12.4	10.5-17.5	3-4
	0.5	20-30	3.5-5.3	5.0-7.4.2	7.0-10.5	2-3

$$\Delta K = 0.7(2S_v)\sqrt{\pi a}$$

Table 4. Small Crack Constant Amplitude Test Summary

Material	Specimen Number	R	Max Stress (ksi)	Vibratory Stress (ksi)	EDM Notch (in)	Half Crack Length Range (c/2, inches)	Delta K Range (ksi(in)**0.5)
Al7075-T73 Forged	A1-3	0.1	45	20.25	0.0095	.0048-.0169	3.5-6.5
	A1-16	0.1	45	20.25	0.005	.0025-.0056	2.5-3.8
	A1-2	0.1	30	13.5	0.0075	.0045-.0229	2.2-5.1
	A1-R6	0.5	24	6	0.0085	.0056-.220	1.1-2.2
	A1-M7	0.5	24	6	0.00875	.0048-.0217	1.0-2.2
Steel 4340 (150 ksi) Forged	S1-2	0.1	70	31.5	0.0077	.0042-.0211	5.1-11.3
	S1-3	0.1	70	31.5	0.0068	.0047-.0217	5.3-11.5
	S1-1	0.5	86	21.5	0.006	.0050-.0224	3.0-6.5
	S3-1	0.5	66	16.5	0.0075	.0061-.0218	3.1-6.0
Ti-6Al-4V Beta STOA Forged	T-13	0.1	80	36	0.0093	.0054-.0183	6.5-12.1
	Ti-4	0.1	67.5	30.4	0.009	.0053-.0218	5.5-11.1
	Ti-6	0.1	70	31.5	0.0084	.0049-.0229	5.4-11.8
	T-20	0.5	80	20	0.0085	.0068-.0238	4.1-7.7
	T-21	0.5	75	18.75	0.0085	.0049-.0226	3.3-7.0
Ti-6Al-4 Alpha-Beta Forged Annealed	1-1038-2A	0.1	45	20.25	0.0085	.0075-.0225	4.3-7.5
	1-1013-1	0.1	50	22.5	0.00985	.0058-.0206	4.2-8.0
	1-1038-5A	0.5	52.5	13.13	0.00875	.0075-.0205	2.8-4.7
	1-1013-3A	0.5	50	12.5	0.008	.0067-.0210	2.5-4.5
Ti-6Al-4V Alpha-Beta Forged Solution Heat Treated & Annealed	1-1037-1	0.1	50	22.5	0.008	.0068-.0228	4.5-8.4
	1-1037-4	0.1	65	29.25	0.0071	.0044-.0230	4.8-11.0
	1-037-5	0.5	60	15	0.008	.0051-.0201	2.6-5.3
	1-037-9	0.5	50	12.5	0.0085	.0065-.0210	2.5-4.5

Table 5. Small Crack Spectrum Test Summary

Material	Specimen Number	Crack Initiation			Crack Propagation		
		EDM Notch (in)	Max Stress (ksi)	R	Max Stress	Half Crack Length Range (c/2, inches)	Total Cycles
Al7075-T73 Forged	Al-M6	0.0078	24	-1	53	.0044-.0204	340179
Steel 4340 (150 ksi) Forged	S1-5	0.0055	70	-1	106	.0049-.020	515424
Ti-6Al-4V Alpha-Beta Forged	T1-12	0.0085	70	-1	106	.0054-.0219	53019
Ti-6Al-4V Alpha-Beta Forged Annealed	1-1013-6	0.0099	55	-1	92	.0055-.0214	220896
Ti-6Al-4V Alpha-Beta Forged Solution Heat Treated and Annealed	1-037-7	0.00685	57.5	-1	92	.0049-.0203	533832

ELASTIC-PLASTIC MODELS FOR MULTI-SITE DAMAGE ¹

Ricardo L. Actis
Engineering Software Research and Development, Inc.
St. Louis, MO

Barna A. Szabó
Center for Computational Mechanics
Washington University, St. Louis, MO

SUMMARY

This paper presents recent developments in advanced analysis methods for the computation of stress intensity factors and the J-integral under conditions of small scale yielding in structural panels with multi-site damage. The method of solution is based on the p-version of the finite element method. Its implementation was designed to permit extraction of linear stress intensity factors using a superconvergent extraction method (known as the contour integral method) and evaluation of the J-integral following an elastic-plastic analysis. Coarse meshes are adequate for obtaining accurate results supported by p-convergence data. The elastic-plastic analysis is based on the deformation theory of plasticity and the von Mises yield criterion.

The model problem consists of an aluminum plate with six equally spaced holes and a crack emanating from each hole. The cracks are of different sizes. The panel is subjected to a remote tensile load. Experimental results are available for the panel. The plasticity analysis provided the same limit load as the experimentally determined load. The results of elastic-plastic analysis were compared with the results of linear elastic analysis in an effort to evaluate how plastic zone sizes influence the crack growth rates. The onset of net-section yielding was determined also. The results show that crack growth rate is accelerated by the presence of adjacent damage, and the critical crack size is shorter when the effects of plasticity are taken into consideration. This work also addresses the effects of alternative stress-strain laws: The elastic-ideally-plastic material model is compared against the Ramberg-Osgood model.

INTRODUCTION

Reliable stress intensity factor computation of cracked structural components is of major importance in modern design of aircraft structures where requirements for residual strength and fatigue crack propagation must be met. In this paper the problem of computing the stress intensity factors for a structural panel with multi-site damage, with guarantee of reliability, is discussed. This work focuses on the accuracy and reliability of the numerical solution of a proposed mathematical model and on the influence that different modeling assumptions may have on the results of the analysis. Two kinds of error are important in this case:

1. The differences between the exact solution of the mathematical problem formulated to represent a physical system or process and its numerical approximation are called errors of discretization. Is it possible to guarantee that the error of discretization is small?

1. Work supported by NASA Lyndon B. Johnson Space Center under Grant NAG 9-622.

2. The differences between the exact solution of the mathematical problem formulated to represent a physical system and the actual response or behavior of the physical system are called errors of idealization or modeling errors. How does incorporating plasticity in the analysis affect the stress intensity factors?

In some cases the two errors, the errors of discretization and modeling, may partially cancel one another. Therefore it is important to verify by means other than the experiment itself, that the numerical solution is close to the exact solution of the model. Only then is it possible to investigate whether the errors of idealization are large or small by making comparisons with experimental observations. The efficient and reliable control of numerical errors, achieved by the use of a superconvergent method for the computation of the stress intensity factors, makes it feasible to investigate the sensitivity of crack extension to alternative modeling decisions.

In this paper, the effect of plasticity on the values of the fracture mechanics parameters is investigated. First, the finite element implementation is discussed; and second the method is illustrated with the integrity assessment of a row of fastener holes with multi-site damage, for which experimental results are available.

FINITE ELEMENT IMPLEMENTATION

Choice of an Extension Process

In the finite element method the control of the errors of discretization can be achieved by mesh refinement (h-extension), by increasing the polynomial degree of elements (p-extension), or a combination of both (hp-extension).

The size of a finite element is the diameter of the smallest circle (or sphere) that contains the element. This diameter is denoted by h and the diameter of the largest finite element in the mesh is denoted by h_{max} . h-Extension involves letting $h_{max} \rightarrow 0$. Alternatively, we can hold the number of elements constant and increase the polynomial degree of elements. The polynomial degree of elements is a vector \mathbf{p} . p-Extension involves letting the smallest polynomial degree $p_{min} \rightarrow \infty$. In hp-extensions mesh refinement is combined with an increase of the polynomial degree of elements. In these processes the number of equations that has to be solved, the number of degrees of freedom, is progressively increased, hence the name 'extension'. Note that h- and p-extensions can be viewed as special cases of hp-extension, which is the general discretization strategy of the finite element method.

An important question is: "Which is the most efficient method of extension with respect to reducing discretization errors?" This question can be answered on the basis of a simple classification of the exact solution of the problem one wishes to solve. The exact solutions (\mathbf{u}_{EX}) have been classified into three main categories:

Category A: \mathbf{u}_{EX} is analytic. A function is analytic at a point if it can be expanded into a Taylor series about that point on the entire solution domain, including the boundaries of the solution domain. Alternatively, the domain can be divided into subdomains and \mathbf{u}_{EX} is analytic on each subdomain, including the boundary of each subdomain. The finite element mesh is so constructed that the boundaries of the subdomains are coincident with element boundaries.

Category B: \mathbf{u}_{EX} is analytic on the entire domain, including the boundaries, with the exception of a finite number of points (in three dimensions \mathbf{u}_{EX} needs not be analytic along a finite number of lines). The mesh is so constructed that the points where \mathbf{u}_{EX} is not analytic are nodal points (in three dimensions the

Figure 4. da/dN For Al7075-T73 Forged, $R = 0.1$

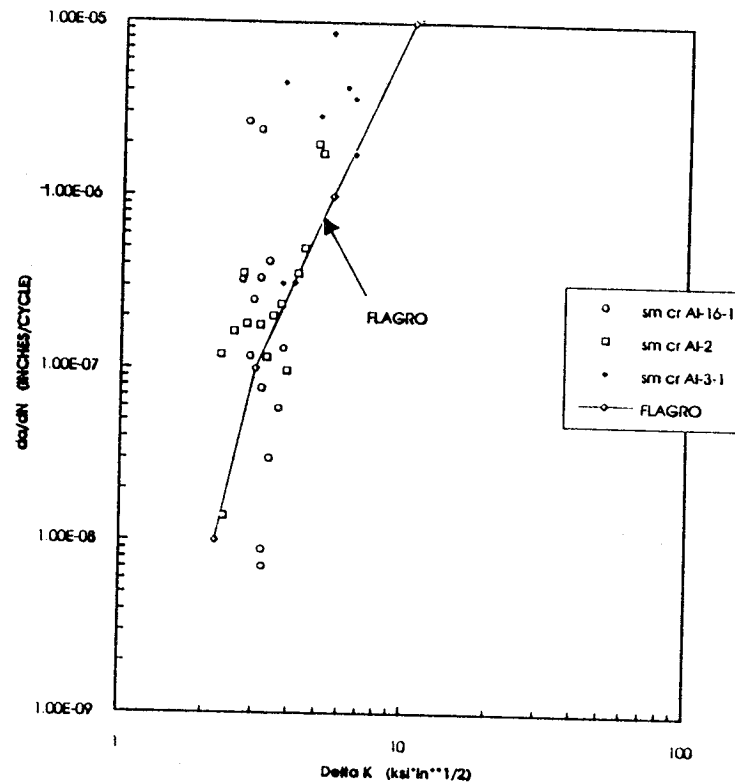


Figure 5. da/dN For 4340 (150 ksi) Steel Forged, $R = 0.1$

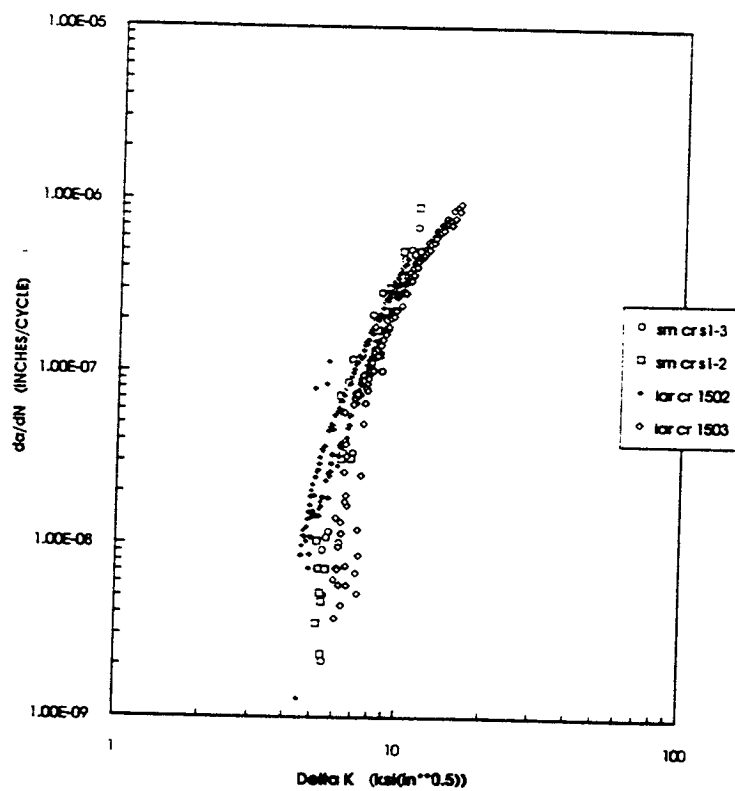


Figure 6. da/dN For Ti-6Al-4V Beta STOA Forged, $R = 0.1$

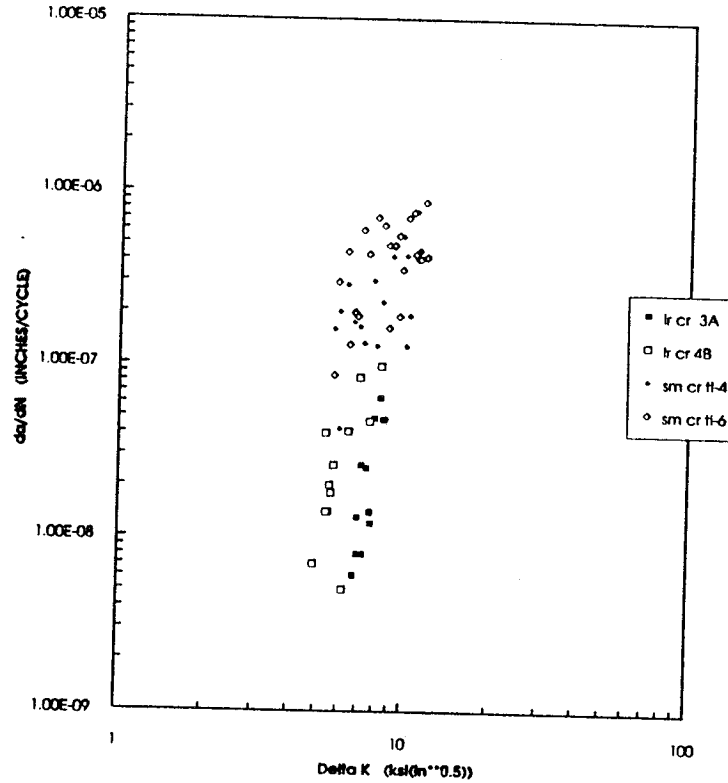


Figure 7. da/dN For Ti-6Al-4V Alpha-Beta Forged, $R = 0.1$

